I&EC research
Industrial & Engineering Chemistry Research

Article

pubs.acs.org/IECR

Model Predictive Control of a Steam Methane Reforming Reactor Described by a Computational Fluid Dynamics Model

Zhe Wu,[†] Andres Aguirre,[†] Anh Tran,[†] Helen Durand,[†] Dong Ni,[‡] and Panagiotis D. Christofides*[,†,¶]

[†]Department of Chemical and Biomolecular Engineering, and [¶]Department of Electrical Engineering, University of California, Los Angeles, California 90095, United States

[‡]College of Control Science and Engineering, Zhejiang University, Hangzhou 310027, China

ABSTRACT: The present work demonstrates, for the first time, the development of a computationally efficient closed-loop system with a model predictive controller (MPC) where a computational fluid dynamics (CFD) process model is utilized to represent the process behavior. Specifically, we present the development of a MPC and its implementation within the CFD model of a steam methane reforming reactor, which has been developed and validated in our previous work, to create the CFD-based closed-loop system. Initially, we develop an MPC algorithm using a linear approximation of the dynamics based on the CFD data, and implement it within the CFD simulation as a user-defined function. The MPC accounts for the physical limitations (maximum allowable operating temperature of the outer reforming tube wall) of the reactor as a constraint. We demonstrate the application of the developed MPC within the CFD simulations for a set-point change under the influence of a tube-side feed disturbance. The CFD model determines an optimal outer reforming tube wall temperature trajectory to track the set-point, and the results of the simulation are compared with those resulting from a CFD-based closed-loop simulation under proportional-integral (PI) control.

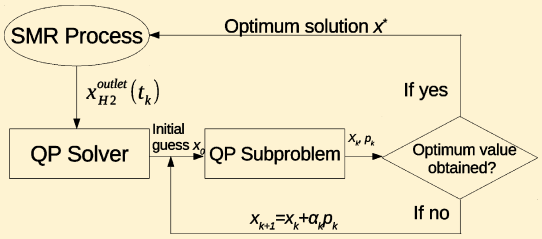

INTRODUCTION

The steam methane reforming (SMR) process is a widely used method for industrial hydrogen production.[1,2] The SMR process converts methane gas and superheated steam in the presence of a nickel-based catalyst into hydrogen, carbon dioxide, and carbon monoxide. The steam methane reformer is the core unit (denoted as "reformer") in the SMR process, and it is composed of a tube side where the SMR process takes place and a furnace side where combustion takes place. The two sides interact by heat transfer through the reforming tube walls. In the furnace side, the combustion of the fuel feed, usually a mixture of methane, hydrogen, carbon dioxide, carbon monoxide, and air, generates heat and provides energy to the reforming tubes primarily by radiative heat transfer.

In the late 1960s, the first mathematical model of a reformer was developed.[3] Reformer mathematical models have become more sophisticated and complex to improve the accuracy with which they represent physical phenomena. As the understanding of physical and chemical phenomena inside the reformer has improved, more comprehensive mathematical models, which consider the physicochemical mechanisms within the reformer (e.g., combustion models, radiation mechanisms, flue gas flow patterns, SMR reaction kinetics, and packed bed reactor models) in more detail, have been developed.[4] However, the increasing complexity of the fundamental nonlinear partial differential equations describing the reformer's physicochemical phenomena[4] makes the mathematical modeling very difficult.

The increases in computing power since the development of the earliest reactor mathematical models have brought new tools to the SMR modeling effort. Computational fluid dyamics (CFD) modeling is a tool which has become increasingly important for reformer modeling and design. CFD combines physical and chemical models with a detailed representation of the reformer geometry, allowing it to generate results which constitute reasonable substitutes for experimental data. Parametric studies conducted using CFD models allow for fast and flexible modification of design parameters without the time and economic expenses associated with physical hardware changes and redesign.[5] Previous studies have successfully simulated industrial furnaces, and also SMR process models as packed bed reactors by means of CFD.[6−12] CFD modeling has also been used to study the physicochemical reforming phenomena at a microscopic scale, for example, the effects of catalyst orientation on catalytic performance,[11] and experimental data validation of a CFD model of a bench-scale reforming tube.[13]

Hydrogen production is dependent on the reforming tube outer wall temperature; that is, a higher outer reforming tube wall temperature, given the same physical operating conditions, should theoretically result in higher hydrogen conversion. However, continuous operation over the design temperature for the reforming tube can result in a decrease in the reforming

Received: January 26, 2017
Revised: April 24, 2017
Accepted: May 3, 2017
Published: May 3, 2017

DOI: 10.1021/acs.iecr.7b00390
Ind. Eng. Chem. Res. 2017, 56, 6002−6011

tube lifetime; that is, a prolonged increase of the tube wall temperature of 20 K over the design temperature decreases the reforming tube's lifetime by half.[4,14] Also, temperatures far enough above the design temperature have the potential to cause catastrophic failure which can result in expensive repairs.[14] As a result, controlling a steam methane reformer with a constrained model-based controller such as model predictive control (MPC) that accounts for the maximum temperature limitations may be beneficial.

Similar processes have been shown to benefit from MPC in the literature (e.g.,[15] evaluates the benefits of MPC compared to classical proportional-integral (PI) control for a gasifier/reformer system using a data-driven model for state predictions within the MPC and a first-principles model to represent the plant), but no work has yet looked at integrating MPC within a CFD model so that the CFD model acts as a representation of the plant dynamics instead of a first-principles model. However, utilizing a CFD model as a representation of the plant dynamics when evaluating controller designs would significantly improve controller assessment at the control design phase compared to using a first-principles model for this purpose. This is because first-principles models are often simplified either by approximating geometry/properties of a plant or by neglecting details of the transport and chemical reaction phenomena occurring inside the plant (e.g., the effects of the flue-gas flow pattern are ignored in ref 4). On the other hand, CFD modeling allows accurate predictions of reacting fluid flow behavior and captures all geometry characteristics of physical systems through computer-aided design software. Thus, simulation data generated from CFD models can often be considered to be reasonable representations of experimental data from the corresponding systems. As a result, if a CFD model can be used to represent the plant in the closed-loop system, process output responses observed for a given resulting control design during a computational investigation are more likely to be consistent with the behavior that will be observed at the plant when it is verified experimentally.

Motivated by this, the present work demonstrates the assembly of a computationally efficient closed-loop system with a model-based feedback controller from a CFD model, model-based controller, and quadratic programing (QP) solver, which can subsequently be simulated by a stand-alone CFD software package (i.e., ANSYS Fluent). Subsequently, the performance of a model-based controller and classical PI controller are compared in terms of set-point tracking and disturbance rejection in the context of an industrial-scale steam methane reforming tube to show the benefits of closed-loop CFD simulations for comparing control design options at the control design phase. The CFD model of a reforming tube used in this study has been developed and validated using published data in Lao et al., and therefore, the reforming tube CFD model can be considered to be a reasonably accurate representation of the plant.[16] Initially, a standard methodology for designing a model-based feedback controller (MPC) by deriving a data-driven discrete-time linear model based on the dynamic open-loop CFD simulation results generated from a high-fidelity CFD model is utilized, so that the MPC computes an optimal temperature trajectory for a reforming tube wall and accounts for the temperature limitations of the reforming tube. Then, we bridge the communication pathway between the reforming tube CFD model and the feedback controller by encoding the MPC algorithm and QP solver in the form of user-defined functions within the ANSYS Fluent framework, which are subsequently integrated into the CFD model to create the closed-loop system. In the closed-loop system, specific information on each component (i.e., the CFD model, feedback model-based controller, and QP solver) becomes accessible by other components, so that the feedback controller can directly retrieve the hydrogen mole fraction at the reforming tube outlet from the CFD simulation data at the end of each sampling period, and the optimized outer wall temperature profile computed based on the MPC algorithm and QP solver can be immediately used as the new boundary condition of the CFD model. The closed-loop system can be simulated by a stand-alone software package ANSYS Fluent, which eliminates the need to establish communication pathways between different software products, reduces the overhead, and decreases the memory requirement for the closed-loop simulation. Finally, CFD-based closed-loop simulations for tracking a set-point change of the area-weighted average hydrogen mole fraction at the outlet of the reforming tube, in the presence of a disturbance, demonstrate the use of the MPC within the CFD simulation, and the results are compared with those of a CFD-based closed-loop simulation under PI control. The CFD simulation results demonstrate the use of closed-loop CFD simulations for determining the most appropriate control design for a given process, showing that the proposed MPC can cause the closed-loop outlet hydrogen mole fraction to approach its set-point more quickly than under PI control because it accounts for the process model and bounds on the control action, and with the addition of an integrating term, it can reject the disturbance.

SINGLE REFORMING TUBE

Industrial-Scale Furnace Geometry. The reforming tube utilized for the CFD-based closed-loop simulations in this work is based on an industrial-scale top-fired, cocurrent reformer designed by Selas Fluid Processing Corporation (Figure 1).

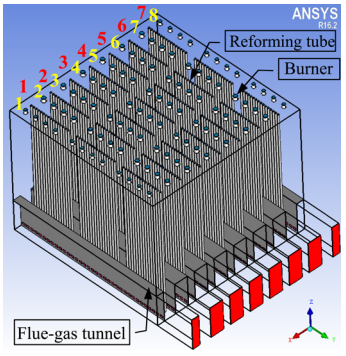

Figure 1. Overall view of furnace geometry.

The reformer is composed of 96 burners distributed across 8 rows of 12 burners, and 336 tubes distributed across 7 rows of 48 tubes. The reforming tubes are packed with nickel oxide over alpha alumina (i.e., Ni/α−Al_2O_3) catalyst particles, which facilitate the reactions within the reformer and heat transfer from the tube walls to the inside of the tube. The external diameter, internal diameter, and exposed length of the reforming tube are 14.6 cm, 12.6 cm, and 12.5 m, respectively.

The reforming tubes are heated mainly by radiation inside the high-temperature furnace chamber to drive the net endothermic SMR reactions. Flue gas tunnels are located at the bottom of the furnace to evacuate the flue gas generated by

DOI: 10.1021/acs.iecr.7b00390
Ind. Eng. Chem. Res. 2017, 56, 6002−6011

the combustion reactions inside the furnace chamber (Figure 1). Plus, there are 35 extraction ports in each of the flue gas tunnels. The furnace flue gas flows through the extraction ports and exits at the front openings of the coffin boxes.

We investigate the implementation of MPC within a CFD model for a single reforming tube[16] in this unit to control the hydrogen production and obtain a desired dynamic response. The single reforming tube is modeled using industrial-scale parameters, including the dimensions and geometry, and the CFD modeling of this tube is summarized in the following sections.

Tube Geometry and Mesh. The mesh quality is especially significant in CFD modeling. Producing a high quality mesh improves solution accuracy using the CFD solver and also decreases computation time. In this work, the reforming tube geometry was simplified to a two-dimensional (2D) axisymmetric geometry (Figure 2a). Using this simplification, we developed a mesh of 100% orthogonal quality with 24 690 quadrilateral cells. This mesh is of significantly higher orthogonal quality and has fewer cells than its equivalent 3D mesh.

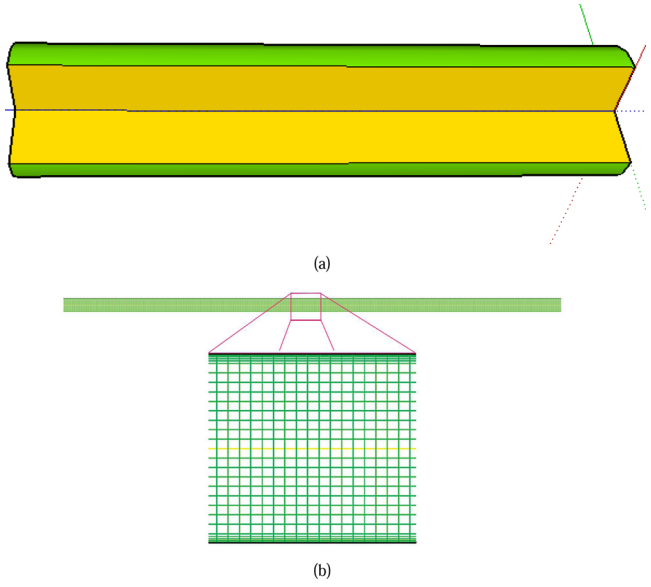

Figure 2. Two-dimensional axisymmetric reforming tube geometry (Figure 2a)and mesh structure (Figure 2b).

Additionally, as discussed in our previous paper,[16] the boundary layer close to the tube wall is specially designed since it plays an important role in modeling heat convection from the inner reforming tube wall to the gas mixture. Specifically, NASA's Viscous Grid Spacing Calculator[17] is adopted with a suitable Y^+ value[18] to calculate the first node height from the inner reforming tube wall.

Kinetic Model. The reforming reactions and water−gas shift reaction take place at the catalyst active sites in the single reforming tube. Specifically, reactants diffuse from the tube-side gas mixture to the catalyst surface, and finally reach the catalyst pores, where the main reactions occur. Then, the products desorb from the catalyst pores and return to the tube-side gas mixture. Due to the complexity of reaction, the following intrinsic reaction kinetic model by Xu and Froment[19] was implemented for the SMR reactions:

$$\mathrm{CH_4}(g) + \mathrm{H_2O}(g) \rightleftarrows \mathrm{CO}(g) + 3\mathrm{H_2}(g),$$

$$r_1 = \frac{k_1}{p_{\mathrm{H_2}}^{2.5}}\left(p_{\mathrm{CH_4}}p_{\mathrm{H_2O}} - \frac{p_{\mathrm{H_2}}^3 p_{\mathrm{CO}}}{K_1}\right)/\mathrm{DEN}^2 \quad (1a)$$

$$\mathrm{CO}(g) + \mathrm{H_2O}(g) \rightleftarrows \mathrm{CO_2}(g) + \mathrm{H_2}(g),$$

$$r_2 = \frac{k_2}{p_{\mathrm{H_2}}}\left(p_{\mathrm{CO}}p_{\mathrm{H_2O}} - \frac{p_{\mathrm{H_2}}p_{\mathrm{CO_2}}}{K_2}\right)/\mathrm{DEN}^2 \quad (1b)$$

$$\mathrm{CH_4}(g) + 2\mathrm{H_2O}(g) \rightleftarrows \mathrm{CO_2}(g) + 4\mathrm{H_2}(g),$$

$$r_3 = \frac{k_3}{p_{\mathrm{H_2}}^{3.5}}\left(p_{\mathrm{CH_4}}p_{\mathrm{H_2O}}^2 - \frac{p_{\mathrm{H_2}}^4 p_{\mathrm{CO_2}}}{K_3}\right)/\mathrm{DEN}^2 \quad (1c)$$

$$\mathrm{DEN} = 1 + K_{\mathrm{CO}}p_{\mathrm{CO}} + K_{\mathrm{H_2}}p_{\mathrm{H_2}} + K_{\mathrm{CH_4}}p_{\mathrm{CH_4}} + K_{\mathrm{H_2O}}p_{\mathrm{H_2O}}/p_{\mathrm{H2}} \quad (1d)$$

where $p_{\mathrm{H_2}}$, $p_{\mathrm{CH_4}}$, $p_{\mathrm{H_2O}}$, p_{CO} and $p_{\mathrm{CO_2}}$ are the partial pressures of H_2, CH_4, H_2O, CO, and CO_2, respectively, in the bulk tube-side gas mixture, $K_{\mathrm{H_2}}$, $K_{\mathrm{CH_4}}$, and K_{CO} are adsorption constants for H_2, CH_4, and CO, respectively, $K_{\mathrm{H_2O}}$ is a dissociative adsorption constant of H_2O, k_1, k_2, and k_3 are rate coefficients of the SMR reactions, and DEN is a dimensionless parameter.

The model of eq 1 was implemented in the ANSYS Fluent simulations by compiling a C language user-defined function (UDF). It is noted that the internal and external diffusion resistances of the catalyst particles are not considered in the above reaction kinetics. Therefore, we multiply the reaction rates in eq 1 by an effectiveness factor, 0.1,[20] to account for the impact of diffusion on the intrinsic reaction rates.

Compressible Gas Flow. The tube-side inlet operating conditions used are those from our previous work.[16] The Mach number is estimated to be larger than 0.3 based on the inlet operating conditions, which means that the density variations of the fluid flow should be taken into consideration because of the high pressure. In this work, we choose the pressure-based solver to apply the pressure-based Navier−Stokes solution algorithm.[18] Compared to the density-based solver, the pressure-based solver has a physical velocity formulation that is utilized in this work for simulating flow through the catalyst packing in the reforming tube, and in addition can obtain the same results as the density-based solver while offering more freedom for the simulations. Additionally, in order to increase the accuracy of the CFD simulation results, the gas equation of state should be selected carefully, especially for the pressure-based solver. Here, the compressible ideal gas equation of state is used to describe the compressibility of the tube-side gas mixture.

Porous Zone. The reforming tube is packed with catalyst particles, which cause a pressure drop that cannot be neglected. Therefore, in this work, the Ergun equation is adopted to estimate the pressure drop across the porous zone in the CFD modeling. The Ergun equation shown in eq 2 is a semiempirical expression which expresses the relationship between the pressure drop and the modified Reynolds number. It can be applied over a wide range of Reynolds numbers and for various packing patterns, and is represented as follows:

DOI: 10.1021/acs.iecr.7b00390
Ind. Eng. Chem. Res. 2017, 56, 6002−6011

$$\frac{\Delta P}{L} = \frac{150\mu}{D_p^2}\frac{(1-\gamma)^2}{\gamma^3}v_\infty + \frac{1.75\rho}{D_p}\frac{(1-\gamma)}{\gamma^3}v_\infty^2 \quad (2)$$

where μ is the viscosity of the fluid, D_p is the mean particle diameter, L is the depth of the porous media, γ is the void fraction (porosity) of the packed bed, ΔP is the pressure drop through the porous media, v_∞ is the bulk velocity of the fluid, and ρ is the density of the porous media. The solution of the Ergun equation (eq 2) is D_p, which can be used to compute the viscous resistance coefficient $(\frac{D_p^2}{150}\frac{\gamma^3}{(1-\gamma)^2})$ and inertial resistance coefficient $(\frac{3.5}{D_p}\frac{1-\gamma}{\gamma^3})$ of the packed bed. We also made the assumption that the viscous and inertial resistance coefficients are defined along the direction vectors in the Cartesian two-dimensional (2D) coordinate system, where the principal axis direction is $v_1 = [1,0]$ and the radius direction is $v_2 = [0,1]$.

For the catalyst particles in the reforming tube, the commercial catalyst, Johnson Matthey's Katalco 23−4Q,[21] a Ni/α−Al_2O_3 catalyst, is adopted in the modeling of the single reforming tube. In our previous work, we discussed the properties of this catalyst and demonstrated that the use of these properties is reasonable for obtaining CFD simulation results in accordance with typical plant data, despite that this catalyst is different from the Ni/$MgAl_2O_4$ catalyst used to derive the reaction kinetics in eq 1.[16]

OPEN-LOOP SIMULATION

In our previous work,[16] a fourth-order polynomial with a given maximum wall temperature (T_{wall}^{max}) was proposed to construct the outer reforming tube wall temperature profile to approximate the plant data.[4] The outer reforming tube wall temperature $T_{wall}(x)$ at the location x (m) from the inlet (x = 0 m) (where the outlet of the tube is x = 12.5 m) can be calculated through the following fourth-order polynomial function:

$$T_{wall}(x) = [x^4 x^3 x^2 x^1 x^0]\begin{bmatrix} -0.0221 \\ 0.8003 \\ -10.734 \\ 64.416 \\ T_{wall}^{max} - 151.83 \end{bmatrix} \quad (3)$$

The value of T_{wall}^{max} in eq 3 can be set using process control to a value that causes a desired hydrogen mole fraction at the outlet of the reforming tube ($\bar{x}_{H_2}^{outlet}$) to be obtained. We demonstrate this method of setting the reforming tube wall temperature profile using an open-loop control strategy. Specifically, the CFD simulations under the open-loop control from ref 16 are first presented to show that $\bar{x}_{H_2}^{outlet}$ can successfully reach the desired set-point $\bar{x}_{H_2}^{set}$ in a disturbance-free environment (Figure 3). In this open-loop simulation, the process manipulated input is a constant predetermined outer reforming tube wall temperature set by eq 3 for the value of T_{wall}^{max} corresponding to $\bar{x}_{H_2}^{set}$ based on the steady-state relationship between $\bar{x}_{H_2}^{outlet}$ and T_{wall}^{max} determined in ref 16. This predetermined profile is shown in Figure 4, and the process output is $\bar{x}_{H_2}^{outlet}$, which changes from an initial steady-state (T_{wall}^{max} = 1100 K, $\bar{x}_{H_2}^{outlet}$ = 0.427) due to the set-point change requiring $\bar{x}_{H_2}^{set}$ = 0.465. It is concluded that we are able to increase $\bar{x}_{H_2}^{outlet}$ to a desired value by raising

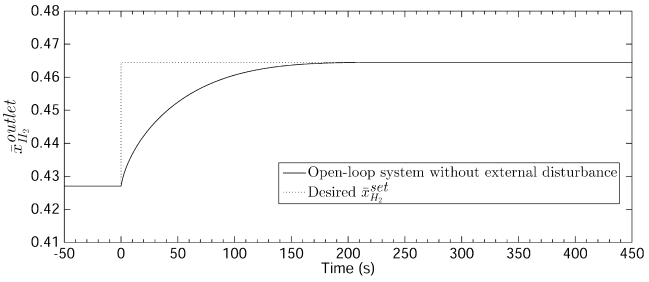

Figure 3. Open-loop dynamic response of $\bar{x}_{H_2}^{outlet}$ using a predetermined outer reforming tube wall temperature trajectory with $\bar{x}_{H_2}^{set}$ = 0.465.

T_{wall} due to the endothermic nature of the SMR process. However, the time required to drive $\bar{x}_{H_2}^{outlet}$ to the desired $\bar{x}_{H_2}^{set}$ under the open-loop policy may not be optimal. Besides, disturbances could also cause the steady-state $\bar{x}_{H_2}^{outlet}$ to deviate from the desired $\bar{x}_{H_2}^{set}$. Thus, in this work, we investigate the manipulation of T_{wall}^{max} using model predictive control (MPC) and comparing the dynamic performance of the algorithm with proportional-integral (PI) and open-loop control.

Remark 1 This work focuses on control and thus the transient response of the process outputs. The CFD data generated by the reforming tube CFD model in which the boundary conditions (i.e., the outer wall temperature and the tube-side feed) are typical plant data have been validated in ref 16 using typical steady-state plant data and have been found to capture very well measurable variables such as species concentration and process-gas temperature at the reforming tube outlet. However, typical transient plant data is not available for evaluating the validity of assumptions made in developing the reforming tube CFD model (e.g., a constant effectiveness factor) when the plant is not operated at a single steady-state but is instead subjected to set-point changes. Nevertheless, the methodology proposed in this work (developing closed-loop CFD simulations for a process under MPC and using them to evaluate MPC versus classical control designs with a simulated plant model that can be considered to be a reasonably accurate representation of experimental data) can be used regardless of the CFD modeling procedure or the process modeled using CFD. Furthermore, the fact that a model considered to be adequate for steady-state CFD simulations may not be appropriate for capturing transient behavior under control designs should be considered when developing a CFD model for industrial processes to ensure that it will accurately represent the plant dynamics for controller evaluation (the availability of routine process operating data at an industrial plant can aid in obtaining the information necessary to validate a CFD model for an industrial facility). Finally, the fact that MPC has the capability to incorporate constraints (unlike classical control designs such as PI control) should not be overlooked when comparing controllers with CFD simulations since it gives the controller flexibility that is not necessarily apparent from the dynamic response that will be observed in the closed-loop CFD simulations.

In practice, T_{wall}^{max} is not set directly, but rather is the result of the transport and chemical reaction phenomena taking place inside the reformer (e.g., the lean combustion phenomena, the redistribution of the combustion heat between the refractory wall, flue gas tunnels, and reforming tubes under the influence of the flue gas flow pattern, and the SMR process). Typically, the optimal outer wall temperature values of reforming tubes

DOI: 10.1021/acs.iecr.7b00390
Ind. Eng. Chem. Res. 2017, 56, 6002−6011

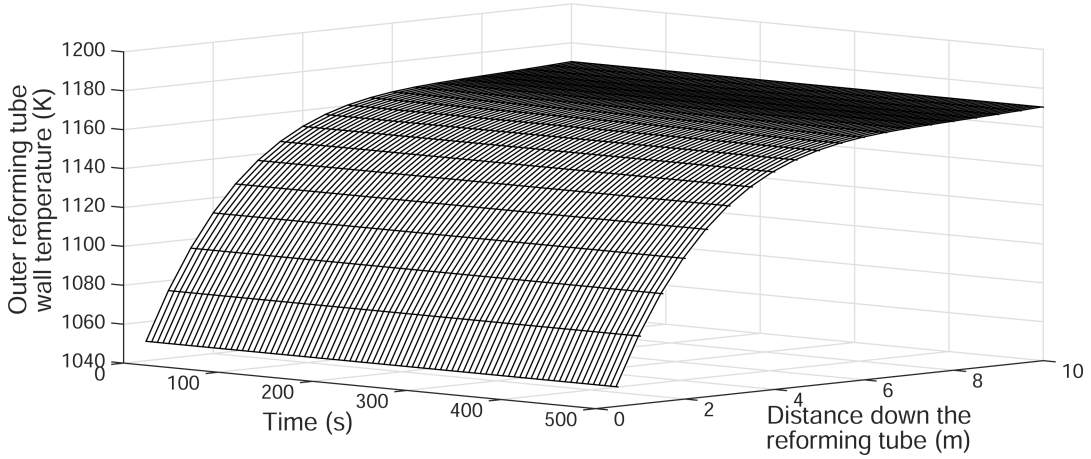

Figure 4. Predetermined outer reforming tube wall temperature trajectory with time for open-loop control with $\bar{x}_{H_2}^{set} = 0.465$.

are achieved by changing the percent opening positions of flow control valves to adjust the distribution of fuel to the reformer, and this operating strategy is often referred to as "furnace balancing" in the literature.[22] In the present work, because we focus on a single reforming tube and thus do not model the burners, we assume that the outer wall temperature can be directly controlled; however, the methodology in this work could be extended to the case that the industrial-scale reformer is simulated (e.g., a control design that regulates the radially averaged value of the hydrogen mole fraction among all reforming tubes by adjusting the burner flow rates with MPC could be developed), though this is not pursued in this work.

DATA-DRIVEN MODELING

To facilitate the use of model predictive control in later sections, data-driven modeling is utilized to derive a linear model from the CFD simulation results that is practical because of its low order but also derived from high-fidelity CFD simulation data. According to the transient response of $\bar{x}_{H_2}^{outlet}$ with a step-change of T_{wall}^{max}, the first-order transfer function from ref 16 is adopted to describe the dynamic response of the output of the reforming tube. It is discussed in ref 16 that the differences among the transfer functions obtained from different step changes are negligible. Therefore, the open-loop simulation results are used to obtain an empirical relationship between $\bar{x}_{H_2}^{outlet}$ and T_{wall}^{max}. Specifically, given a set of T_{wall}^{max} and $\bar{x}_{H_2}^{outlet}$ data with time from the open-loop simulation, the maximum likelihood estimation (MLE)[23,24] method is first used to identify the parameters of the single-input−single-output (SISO) model. Then, the SISO model is converted to a discrete-time state-space model for use in MPC. The SISO model and MLE formulation are:

$$y(k) = \frac{B(s)}{A(s)}u(k) + \frac{1}{A(s)}e(k) \tag{4a}$$

$$\begin{cases} A(s) = a_0 + a_1 s \\ B(s) = b_0 \end{cases}$$

$$\tau(y(k), u(k)) = \arg\max_{\theta\in\Theta}\{y(k)|u(k), \theta\} \tag{4b}$$

where $y(k)$ and $u(k)$ are deviation variables for the process output $\bar{x}_{H_2}^{outlet}$ and process input T_{wall}^{max}, respectively, $e(k)$ is the measurement error, which is assumed to be a white noise function with zero mean and a standard deviation of 1, $A(s)$ and $B(s)$ are the coefficients of the process input and measurement error on the Laplace domain, k is a discrete point at which the system is being evaluated, $\tau(y(k),u(k))$ is the maximum likelihood estimator, and $\theta = [a_0\ a_1\ b_0]$ is the parameter vector of the estimated model.

The SISO model (eq 4a) is then converted to a discrete-time state-space model to represent the process model in MPC. Disregarding measurement error in the SISO model, the following discrete-time state-space model is obtained via Matlab functions:

$$\begin{cases} x_{d,k+1} = \mathbf{A}x_{d,k} + \mathbf{B}u_k \\ y_k = \mathbf{C}x_{d,k} + \mathbf{D}u_k \end{cases} \tag{5}$$

where $x_{d,k}$ is the current state of the discrete-time system, $x_{d,k+1}$ is the next state of the system with respect to the current state $x_{d,k}$ and input u_k, y_k is the process output, and **A**, **B**, **C**, and **D** are the coefficient matrices corresponding to the estimated coefficients in the SISO model. Given the MPC sampling period $\Delta T = 10.0$ s, the coefficient matrices **A**, **B**, **C**, and **D** in eq 5 are estimated to be 0.774, 1.83×10^{-4}, 1.00, and 0.00, respectively. Therefore, a data-driven model that describes the dynamic response of $\bar{x}_{H_2}^{outlet}$ is obtained for the purpose of designing MPC.

FEEDBACK CONTROLLER DESIGN

In this section, an MPC is developed and incorporated within CFD-based closed-loop simulations to control $\bar{x}_{H_2}^{outlet}$ to attain the new desired set-point $\bar{x}_{H_2}^{set}$. The closed-loop system under this feedback control scheme is able to eliminate the offset between $\bar{x}_{H_2}^{outlet}$ and $\bar{x}_{H_2}^{set}$ at steady-state, and also to enhance the dynamic performance of the process. Specifically, given an increase of $\bar{x}_{H_2}^{set}$ at a certain time, it is observed that under the feedback control scheme, $\bar{x}_{H_2}^{outlet}$ initially approaches the desired $\bar{x}_{H_2}^{set}$ rapidly due to a large increase in the maximum wall temperature (and thus in the wall temperature distribution according to eq 3). After the initial fast increase of the temperature, the outer reforming tube wall temperature drops somewhat. As a result, $\bar{x}_{H_2}^{outlet}$ increases less quickly in this period, and finally approaches $\bar{x}_{H_2}^{set}$ slowly and maintains $\bar{x}_{H_2}^{outlet}$ at

DOI: 10.1021/acs.iecr.7b00390
Ind. Eng. Chem. Res. 2017, 56, 6002−6011

the final steady-state. Closed-loop simulation results under PI control, presented for comparison, show similar behavior. A disturbance is also considered, and the MPC must be augmented by integral action to avoid set-point offset during closed-loop simulation due to the approximate model used for state predictions. Assumptions made in the controller designs are that the dynamics of the outer reforming tube wall temperature can be neglected (in other words, we can assume that the outer reforming tube wall temperature is able to reach the predicted profile immediately). In addition, we assume that the measurements of $\bar{x}_{H_2}^{outlet}$ are available at all sampling instances.

Considering the safety requirements and life expectancy of the reforming tube for practical hydrogen production, the constraint on T_{wall}, which is the maximum allowable temperature value of 1200 K, is added to all control schemes investigated in this section. Specifically, temperature limits are imposed as hard constraints within the MPC optimization problem to ensure that the controller output never exceeds the limit. In the PI control scheme design, the temperature constraints are activated if the controller output (T_{wall}^{max}) is out of the range. The specific PI and MPC schemes used are presented in the following sections.

PI Control. The PI control scheme was developed in our previous work[16] as follows:

$$e(t_k) = \bar{x}_{H_2}^{set} - \bar{x}_{H_2}^{outlet}(t_k) \tag{6a}$$

$$u_{PI}(t_k) = K_c\left(e(t_k) + \frac{1}{\tau_I}\int_{t_0}^{t_k} e(\tau)\,d\tau\right) \tag{6b}$$

$$T_{wall}^{max}(t_k + \Delta t) = T_{wall}^{max}(t_0) + u_{PI}(t_k) \tag{6c}$$

$$\text{s.t.} \quad T_{wall}(x, t_k + \Delta t) \le T_{max} \tag{6d}$$

where t_k, t_0, and Δt are the current time, the initial time, and the sampling period, respectively. The error $e(t_k)$ between a measurement of $\bar{x}_{H_2}^{outlet}(t_k)$ and the set-point $\bar{x}_{H_2}^{set}$ is represented by eq 6a. T_{max} is the upper bound of the outer reforming tube wall temperature, $T_{wall}^{max}(t_0)$ is the maximum outer reforming tube wall temperature at the initial steady-state, and $T_{wall}^{max}(t_k + \Delta t)$ is the predicted value for the beginning of the next sampling period. K_c and τ_I are the controller gain and controller time constant of the controller output $u_{PI}(t_k)$ in eq 6c. Parameters of the classical PI controller are calculated as follows: initial estimates of K_c and τ_I are computed based on the Cohen−Coon tuning method and the SISO data-driven model, and then are adjusted until the process response of the CFD closed-loop system appears to be critically damped, and their values are found be to K_c = 1856.3 and τ_I = 46.4, which provides a fast response without overshoot. The PI sampling period is set to 0.04 s, based on the previous work.[16]

At each sampling time, the controller output $u_{PI}(t_k)$ is computed based on the deviation of the current $\bar{x}_{H_2}^{outlet}$ from its set-point $\bar{x}_{H_2}^{set}$. After applying the controller output $u_{PI}(t_k)$, the predicted wall temperature $T_{wall}^{max}(t_k + \Delta t)$ is attained. If $T_{wall}^{max}(t_k + \Delta t)$ is greater than the maximum temperature, then the value of $T_{wall}^{max}(t_k + \Delta t)$ is set to T_{max} (eq 6d). This predicted wall temperature profile (eq 3) will be applied to the process during the next sampling period. The above procedure is repeated until the error between $\bar{x}_{H_2}^{outlet}$ and $\bar{x}_{H_2}^{set}$ is smaller than the specified tolerance.

Model Predictive Control Scheme. On the basis of the data-driven modeling of the reaction process in a single reforming tube, a model predictive controller is designed to regulate the hydrogen production at the outlet of the tube. Minimizing the sum of the deviations of $\bar{x}_{H_2}^{outlet}$ from its desired set-point $\bar{x}_{H_2}^{set}$ throughout the prediction horizon is chosen as the controller objective function, and the outer reforming tube wall temperature is used as the manipulated input. The formulation of the MPC is

$$\min_{T_{wall}^{max}(j), j=1,\ldots,P} \sum_{i=1}^{P} (y_{k+i} - r_{sp})^T Q_i (y_{k+i} - r_{sp}) \tag{7a}$$

$$\text{s.t.} \quad x_{d,k+m+1} = \mathbf{A}x_{d,k+m} + \mathbf{B}u_{k+m}$$
$$m = 0, \ldots, P-1 \tag{7b}$$

$$y_{k+m} = \mathbf{C}x_{d,k+m} + \mathbf{D}u_{k+m}$$
$$m = 0, \ldots, P \tag{7c}$$

$$T_{wall}(x, t_k + \Delta T) \le T_{max} \tag{7d}$$

where y_{k+i} is the deviation variable for the predicted process output $\bar{x}_{H_2}^{outlet}$ at i sampling steps from the current (kth) sampling step within the prediction horizon, r_{sp} is the deviation form of the desired set-point $\bar{x}_{H_2}^{set}$, t_k is the current time, P = 20 is the number of prediction steps in the horizon, and Q_i is a penalty matrix, which is set to the identity matrix here. The notation $T_{wall}^{max}(j)$, j = 1, ..., P, signifies the P maximum wall temperatures computed throughout the prediction horizon by the MPC algorithm. The MPC of eq 7 is implemented with a sampling period ΔT = 10.0 s and a prediction horizon $P\Delta T$ = 200.0 s (the control horizon is the same as the prediction horizon). It is noted that the MPC sampling period is different from the PI sampling period, because we chose the MPC sampling period in accordance with practical industrial considerations such that the MPC computes a new control action less frequently than the PI control law. Additionally, the CFD-based closed-loop simulation results with several different prediction horizons were compared as will be shown below, and the chosen prediction horizon was shown to provide reasonable results with a reasonable computation time.

At the end of each MPC sampling period, the measurement of $\bar{x}_{H_2}^{outlet}$ is acquired from the CFD-based closed-loop simulation for the calculation of the optimal solution of eq 7. Then, the first value of the set of optimal T_{wall}^{max} determined for each sampling period in the prediction horizon is applied to the system over the following sampling period. The above procedure is repeated with new measurements at every sampling time.

The MPC is implemented within the CFD software package Fluent utilized for the simulations through a user-defined function (UDF). Fluent UDF's cannot directly compile Matlab programs, and the data exchange between the two software packages is time-consuming; thus, Matlab was not utilized to implement MPC within the CFD-based closed-loop simulations. Instead, we developed an MPC inside the UDF by using an active-set method[25,26] to deal with the inequality-constrained quadratic programming (QP) problem in MPC. A standard QP has the following form (where the active set is denoted):

DOI: 10.1021/acs.iecr.7b00390
Ind. Eng. Chem. Res. 2017, 56, 6002−6011

$$\min_x q(x) = \frac{1}{2}x^{\mathrm{T}}Gx + x^{\mathrm{T}}d \tag{8a}$$

$$\text{s.t.} \quad a_i^{\mathrm{T}}x \le b_i, \quad i \in \mathcal{A}(x^*) \tag{8b}$$

where $\mathcal{A}(x)$ is an active set, x^* is the optimal solution of the QP, and a_i and b_i are vectors used in the inequality constraints. Equation 7 is of the form of eq 8 upon substitution of the model of eq 5 into the objective function of eq 7 so that the active-set method can be applied. The active-set method calculates the optimal solution by iteratively solving equality-constrained QP subproblems, which are formulated as follows:

$$\begin{bmatrix} G & a_{i,k}^{\mathrm{T}} \\ a_{i,k} & 0 \end{bmatrix}\begin{bmatrix} -p_k \\ \lambda^* \end{bmatrix} = \begin{bmatrix} d + Gx_k \\ a_{i,k}x_k - b_{i,k} \end{bmatrix} \tag{9}$$

$$\alpha_k \overset{\text{def}}{=} \min\left(1, \min_{i \notin \mathcal{W}_k, a_i^T p_k \le 0} \frac{b_i - a_i^T x_k}{a_i^T p_k}\right) \tag{10a}$$

$$x_{k+1} = x_k + \alpha_k p_k \tag{10b}$$

where G and d are matrices specific to the QP developed for a given process model (eq 8), λ^* is a Lagrange multiplier, $\mathcal{W}_k$ is the working set, α_k is the step-length coefficient, p_k is the step length, $a_{i,k}$ is a matrix with row vectors a_i^{T} where $i \in \mathcal{W}_k$, $b_{i,k}$ is a vector with components b_i, $i \in \mathcal{W}_k$, x_k is the current solution, and x_{k+1} is the solution for the next iteration. Specifically, given x_k and a working set $\mathcal{W}_k$, a step p_k is computed through eq 9 by treating all the constraints in $\mathcal{W}_k$ as equalities, and temporarily disregarding the others until eq 8 is minimized. Then, through eq 10a, α_k is determined, and therefore x_{k+1} is derived for the next iteration using eq 10b. The subproblems are iteratively solved until the optimal point x^* is derived that satisfies all the constraints as shown in Figure 5. We validated this QP solver

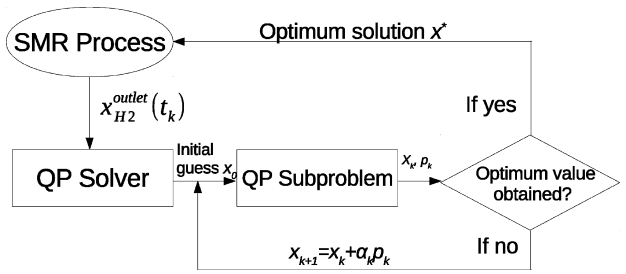

Figure 5. MPC closed-loop system with QP solver, in which QP subproblems are solved iteratively to obtain the optimal solution.

programmed within the UDF by comparing results from solving the QP with the results from the Matlab QP-solving function, and found the difference to be negligible.

Remark 2. Having the data-driven model derived from high-fidelity CFD data for designing the MPC is beneficial compared to having a first-principles model for developing such a controller because the CFD data used to obtain the model is likely to be a better representation of the data that would be obtained from an online process than the data obtained from a first-principles model would be. This means that the MPC designed from such a model may be able to be implemented online without the need to utilize process operating data to develop a model for the MPC as would be typical, or if a data-driven model is obtained from routine operating data, the response of the process operated under the MPC with the process data-based data-driven model may be similar to that expected based on the closed-loop CFD simulations with the CFD-based data-driven model.

Remark 3. In this work, we focus on a single reforming tube and therefore the process output measurement that is fed back to the MPC is the radially averaged mole fraction of hydrogen at the outlet of the reforming tube. This quantity is not typically measured in practice because at a hydrogen production plant, there are many reformers and the hydrogen mole fraction in the combined gas obtained from all reforming tubes would be measured. However, if the method described in this paper were extended to an online reformer, the data-driven model could capture the dynamics between the burner flow rates and the hydrogen mole fraction in the combined gas from all reforming tubes, for example, in which case the measured output could be readily obtained.

MPC and Integral Feedback Control Scheme. Since our MPC is developed based on a data-driven model, which cannot account for changes of the process model when disturbances are introduced to the process, an MPC and integral feedback control scheme is designed to maintain good dynamic performance of the closed-loop system in the presence of disturbances. The controller is formulated as follows:

$$u_{\mathrm{MPC}+I}(t_k) = u_{\mathrm{MPC}}(t_k) + u_I(t_k) \tag{11a}$$

$$u_I(t_k) = \frac{K_c}{\tau_I}\int_{t_0}^{t_k} e(\tau)\,\mathrm{d}\tau \tag{11b}$$

where $u_{\mathrm{MPC}+I}(t_k)$, $u_{\mathrm{MPC}}(t_k)$ and $u_I(t_k)$ are the controller output, the term in the controller output calculated by the MPC of eq 7, and the term in the controller output calculated by the integration in eq 11b, respectively. The controller gain for the integration $(\frac{K_c}{\tau_I})$ as shown in eq 11b is chosen as 12 based on closed-loop simulations that indicated that this value prevented overshoot and offset from the set-point in the simulation of the closed-loop system. It is noted that this strategy is different from the dynamic optimization and integral feedback control scheme examined in ref 16 because the value $u_{\mathrm{MPC}}(t_k)$ in eq 11a is determined from eq 7 utilizing feedback at each sampling time, while a similar term in the dynamic optimization and integral feedback control scheme from the prior work was determined at the first sampling period in the prediction horizon but not updated with feedback throughout time because the MPC was not incorporated within the UDF in ref 16.

Results. In this section, we present process responses of the closed-loop systems with the classical PI controller and MPC, both in the presence and absence of disturbances, for the reforming tube. Each closed-loop system is fully constructed under the ANSYS Fluent framework and is composed of two major components (i.e., the reforming tube CFD model and feedback controller), which are sequentially executed. The feedback controller is realized in the form of a user-defined function of the CFD model as shown in eqs 6 and 7, so that the direct communication between the CFD model and feedback controller can be established. Dynamic simulations of the closed-loop reforming tube CFD model with feedback control were executed by the ANSYS Fluent solver on an 8 core 32 RAM PC with 1TB internal storage. Typically, the solution time of each simulation is expected to decrease with more computational resources (e.g., the ANSYS Fluent solver utilizes

DOI: 10.1021/acs.iecr.7b00390
Ind. Eng. Chem. Res. 2017, 56, 6002−6011

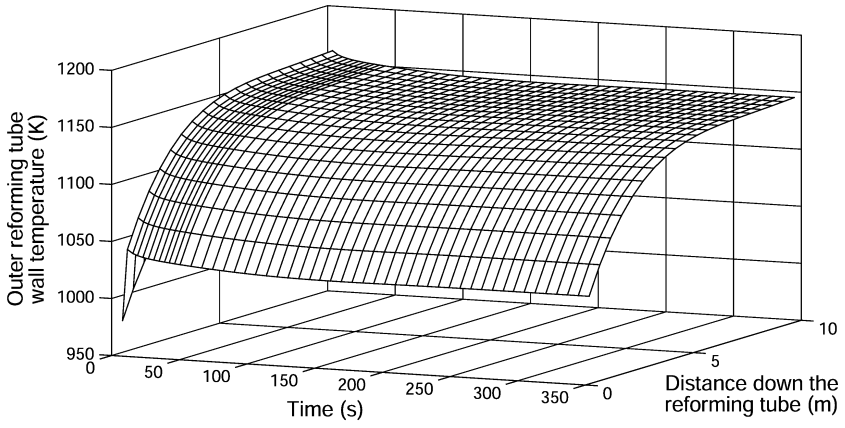

(a)

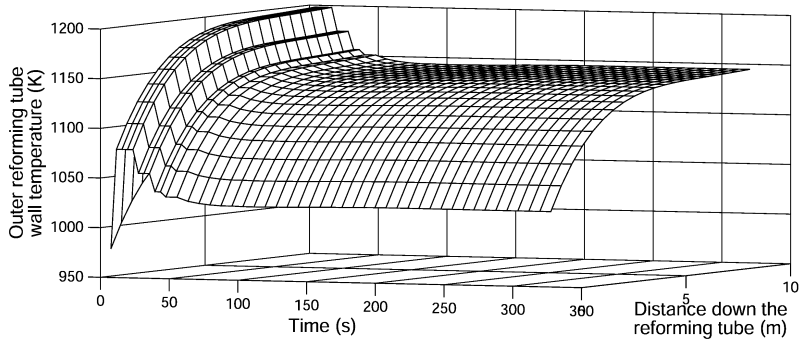

(b)

Figure 6. Outer reforming tube-wall temperature profile trajectory in the absence of a tube-side feed disturbance under PI control (a) and under MPC (b) with $\bar{x}_{H_2}^{set} = 0.465$.

more computing nodes), which was observed when the ANSYS Fluent solver was changed from serial mode (i.e., 1 computing node) to 4-core parallel mode (i.e., 4 computing nodes). However, as the number of computing nodes increases, the overhead due to communication between the computing nodes also increases, which eventually negates the benefit of parallel computing. In the present work, the reduction in solution time has been found to be negligible when the ANSYS Fluent solver is allowed to utilize more than 4 computing nodes, and the 4-core parallel ANSYS Fluent solver typically takes 24 h of computational time to simulate 100 s in the closed-loop system. In addition, the simulation settings of the closed-loop systems are the same as in the open-loop simulation. Specifically, in each simulation, the process was initiated from an initial steady-state under a constant wall temperature profile (i.e., T_{wall}^{max} = 1100 K, $\bar{x}_{H_2}^{outlet} = 0.427$). After that, a set-point change ($\bar{x}_{H_2}^{set}$ = 0.465) is introduced to the closed-loop system to test its dynamic performance.

The closed-loop simulations under PI control and under MPC were run for about 350 s to allow $\bar{x}_{H_2}^{outlet}$ to reach its final steady-state. Figure 6 panels a and b show that the predicted outer reforming tube wall temperature profiles under the two control schemes are within the temperature constraints. Figure 7 compares the dynamic performance of $\bar{x}_{H_2}^{outlet}$ with the same step-change in the set-point $\bar{x}_{H_2}^{set}$ for the two controllers. The simulations show that the model predictions within the MPC allowed it to achieve a rapid dynamic response to minimize the objective function and track the set-point.

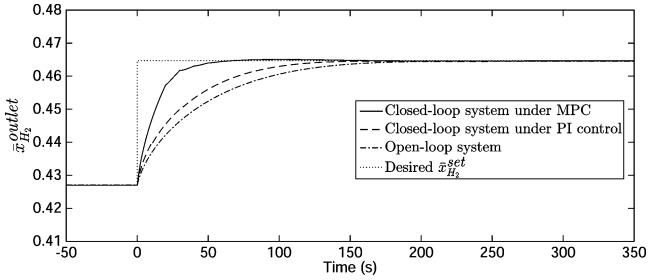

Figure 7. Propagation of $\bar{x}_{H_2}^{outlet}$ with time in the absence of a tube-side feed disturbance under MPC (solid line) and under PI control (dashed line). The open-loop system response (dashed-dotted line) is also included for a wall temperature profile for which $\bar{x}_{H_2}^{set} = 0.465$.

In addition to evaluating the performance of the closed-loop reforming tube under MPC, we also investigated the use of CFD-based closed-loop simulations in tuning the MPC sampling period and prediction horizon. Several MPC closed-loop simulations with various prediction horizons (i.e., P = 10, P = 30) and the same MPC sampling period (ΔT = 10 s) were compared with results from the values chosen in this work (P = 20, ΔT = 10 s). The dynamic responses of the closed-loop MPC with the three different prediction horizons are similar, and the prediction horizon P = 30 requires a longer simulation time than the two others. Even though the MPC closed-loop simulations utilizing P = 10 and P = 20 have almost the same performance, P = 20 is selected based on the tuning method for the prediction horizon since P = 20 is most likely to cover the

DOI: 10.1021/acs.iecr.7b00390
Ind. Eng. Chem. Res. 2017, 56, 6002−6011

entire dynamic response. In addition, MPC closed-loop simulations with different MPC sampling periods (i.e., ΔT = 20 s, ΔT = 30 s) and the same prediction horizon (P = 20) were also conducted and the results are compared in Figure 8,

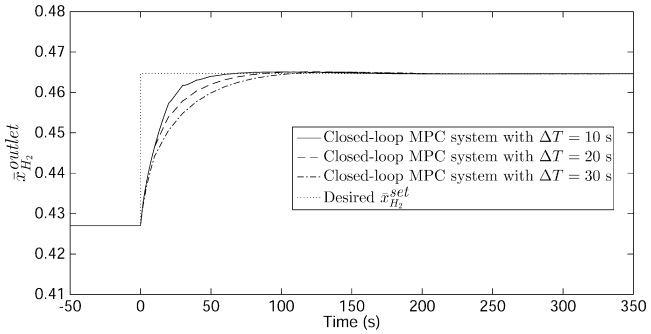

Figure 8. Propagation of $\bar{x}_{H_2}^{outlet}$ with time in the absence of a tube-side feed disturbance under MPC with different MPC sampling periods (i.e., ΔT = 10 s, ΔT = 20 s, ΔT = 30 s) in which $\bar{x}_{H_2}^{set}$ = 0.465.

which exhibit noticeable distinctions in the simulation results. It is noticed that the three MPC's with different sampling periods were all able to drive the value of $\bar{x}_{H_2}^{outlet}$ to its set-point without offset; however, the dynamic response improved as the MPC sampling period ΔT was decreased. Hence, ΔT = 10 s is a reasonable choice for the sampling period of the MPC.

CFD-based closed-loop simulations were also performed in the presence of a 20% disturbance in the tube-side feed mass flow rate. In this case, the MPC of eq 7 was not able to achieve successful set-point tracking due to the plant-model mismatch, and the proposed MPC and integral feedback control (MPC+I) scheme shown in eqs 11a and 11b was used. The fraction, K_c/τ_I, of the MPC+I scheme was chosen based on a trial-and-error approach such that the closed-loop simulation, in which the SISO model was used to represent the process dynamics, under the influence of the disturbance appeared to be critically damped. The results of utilizing this control scheme, as well as PI and open-loop control, are shown in Figure 9. Both the MPC and integral feedback control scheme and the PI controller were able to eliminate the impact of the disturbance, and to successfully drive $\bar{x}_{H_2}^{outlet}$ to the desired $\bar{x}_{H_2}^{set}$. The results also suggest that CFD-based closed-loop simulations may be valuable for evaluating whether a proposed controller design,

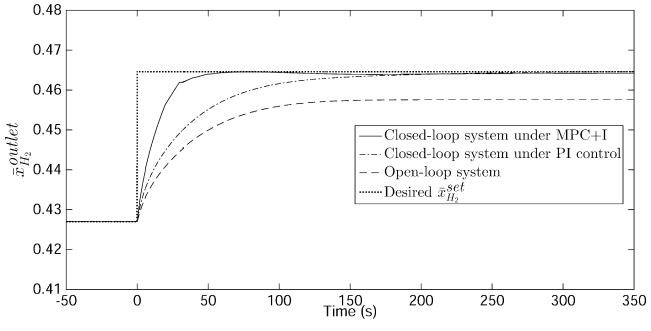

Figure 9. Propagation of $\bar{x}_{H_2}^{outlet}$ with time in the presence of a 20% tube-side feed disturbance under the MPC and integral feedback control scheme (solid line) and under PI control (dashed-dotted line). The open-loop system response (dashed line) is also included for a wall temperature profile for which $\bar{x}_{H_2}^{set}$ = 0.465.

particularly when an empirical model is used in deriving the controller, will provide adequate control (e.g., disturbance rejection) for a process.

Comparison between Control Schemes. We compare the performance of the PI and MPC feedback control schemes through two primary aspects: the ability to drive $\bar{x}_{H_2}^{outlet}$ to the desired $\bar{x}_{H_2}^{set}$ in the presence of a step change in set-point, and the speed of the closed-loop response. Through the comparison between PI and MPC, we observe that both controllers can successfully drive $\bar{x}_{H_2}^{outlet}$ to $\bar{x}_{H_2}^{set}$ without offset. Nevertheless, there are differences between the predicted outer reforming tube wall temperature trajectories. Specifically, the MPC feedback control scheme initially maintains T_{wall}^{max} at the maximum allowable temperature 1200 K for 20 s as shown in Figure 6b, which causes $\bar{x}_{H_2}^{outlet}$ to rapidly increase toward the desired $\bar{x}_{H_2}^{set}$. It takes only 60 s for $\bar{x}_{H_2}^{outlet}$ to reach the desired $\bar{x}_{H_2}^{set}$ for the first time, while it takes around 308 s for the PI control scheme. Therefore, the improvement of the dynamic response is nearly 80.5%. In addition, it is noticed that there exists a slight overshoot ($\bar{x}_{H_2}^{outlet}$ = 0.4651) compared to the desired set-point ($\bar{x}_{H_2}^{set}$ = 0.465) under the MPC scheme, but this overshoot is small (it is only 0.3% of the total difference between the initial condition and set-point of $\bar{x}_{H_2}^{outlet}$). With regard to the settling time, the closed-loop system under MPC takes ~250 s to advance to the new steady-state, which is on the same order of magnitude as the time required for the system under the PI controller for which it takes ~308 s. The closed-loop system with the MPC achieves a faster response than the one with the PI controller because the closed-loop system with the MPC has the knowledge of the process dynamics, which allows it to calculate more aggressive control actions.

■ CONCLUSION

The present work detailed the integration of a model predictive controller with a reforming tube CFD model to represent an industrial-scale single reforming tube to develop a computationally efficient closed-loop system. The development of a SISO data-driven model, MPC and QP solver were discussed. Specifically, the MPC formed a quadratic program due to the use of an approximate linear model developed based on the dynamic CFD simulation data generated from open-loop simulations of the reforming tube CFD model. Furthermore, the MPC was formulated to account for a physical constraint on the reforming tube (an upper limit on the tube wall temperature) utilizing a hard constraint in the optimization problem. Then, the MPC algorithm and QP solver were encoded in the form of user-defined functions under the ANSYS Fluent framework and were subsequently integrated into the CFD model to create the CFD-based closed-loop system. Closed-loop systems were simulated by ANSYS Fluent, which allowed direct communication between the MPC algorithm, QP solver, and the CFD model, which reduced the overhead and decreased the memory requirement for the closed-loop simulation. It is important to point out that this unified CFD modeling/feedback control framework can be applied to other chemical process systems where CFD modeling is needed to capture process behavior. Dynamic CFD simulation data was used to compare MPC and PI controller designs and to evaluate the best parameters (sampling period and prediction horizon) for the MPC. The

DOI: 10.1021/acs.iecr.7b00390
Ind. Eng. Chem. Res. 2017, 56, 6002−6011

simulations indicated that the settling time of the closed-loop system with the MPC is shorter than the one with the PI controller in the absence and presence of disturbances, which confirmed that the MPC offered superior set-point tracking and disturbance rejection than the classical PI controller, assuming that the reforming tube CFD model that was rigorously validated with typical steady-state plant data provides an accurate representation of the process dynamics during the transients induced by set-point changes. In future work, the MPC could be modified with additional constraints on the rate of change of the outer wall temperature to produce practically implementable control actions accounting for limitations of the actuation system, and could be extended to control an industrial-scale reformer.

AUTHOR INFORMATION

Corresponding Author

*E-mail: pdc@seas.ucla.edu.

ORCID

Panagiotis D. Christofides: 0000-0002-8772-4348

Notes

The authors declare no competing financial interest.

ACKNOWLEDGMENTS

Financial support from the U.S. Department of Energy is gratefully acknowledged.

REFERENCES

(1) Amirshaghaghi, H.; Zamaniyan, A.; Ebrahimi, H.; Zarkesh, M. Numerical simulation of methane partial oxidation in the burner and combustion chamber of autothermal reformer. *Applied Mathematical Modelling* **2010**, *34*, 2312−2322.

(2) Sadooghi, P.; Rauch, R. Pseudo heterogeneous modeling of catalytic methane steam reforming process in a fixed bed reactor. *J. Nat. Gas Sci. Eng.* **2013**, *11*, 46−51.

(3) McGreavy, C.; Newmann, M. W. Development of a mathematical model of a steam methane reformer. *Proceedings of the Conference on Industrial Applications of Dynamic Modelling*; Institution of Electrical Engineers: Durham, England, 1969.

(4) Latham, D.Mathematical Modeling of An Industrial Steam Methane Reformer. Master's Thesis, Queen's University, 2008.

(5) Uriz, I.; Arzamendi, G.; Diéguez, P. M.; Gandía, L. M. In *Renewable Hydrogen Technologies: Production, Purification, Storage, Applications and Safety*; Gandía, L. M., Arzamendi, G., Diégues, P. M., Eds.; Elsevier: Oxford, UK, 2013; pp 401−435.

(6) Baburić, M.; Duić, N.; Raulot, A.; Coelho, P. J. Application of the conservative discrete transfer radiation method to a furnace with complex geometry. *Numer. Heat Transfer, Part A* **2005**, *48*, 297−313.

(7) Han, Y. L.; Xiao, R.; Zhang, M. Y. Combustion and pyrolysis reactions in a naphtha cracking furnace. *Chem. Eng. Technol.* **2006**, *30*, 112−120.

(8) Stefanidis, G. D.; Merci, B.; Heynderickx, G. J.; Marin, G. B. CFD simulations of steam cracking furnaces using detailed combustion mechanisms. *Comput. Chem. Eng.* **2006**, *30*, 635−649.

(9) Noor, M. M.; Wandel, A. P.; Yusaf, T. Detail guide for CFD on the simulation of biogas combustion in bluff-body mild burner. *Proceedings of the International Conference on Mechanical Engineering Research*; Institute of Physics Publishing, 2013; pp 1−25.

(10) Calis, H. P. A.; Nijenhuis, J.; Paikert, B. C.; Dautzenberg, F. M.; van den Bleek, C. M. CFD modelling and experimental validation of pressure drop and flow profile in a novel structured catalytic reactor packing. *Chem. Eng. Sci.* **2001**, *56*, 1713−1720.

(11) Dixon, A. G. CFD study of effect of inclination angle on transport and reaction in hollow cylinder catalysts. *Chem. Eng. Res. Des.* **2014**, *92*, 1279−1295.

(12) Guardo, A.; Coussirat, M.; Larrayoz, M. A.; Recasens, F.; Egusquiza, E. CFD flow and heat transfer in nonregular packings for fixed bed equipment design. *Ind. Eng. Chem. Res.* **2004**, *43*, 7049−7056.

(13) Behnam, M.; Dixon, A. G.; Wright, P. M.; Nijemeisland, M.; Stitt, E. H. Comparison of CFD simulations to experiment under methane steam reforming reacting conditions. *Chem. Eng. J.* **2012**, *207−208*, 690−700.

(14) Pantoleontos, G.; Kikkinides, E. S.; Georgiadis, M. C. A heterogeneous dynamic model for the simulation and optimization of the steam methane reforming reactor. *Int. J. Hydrogen Energy* **2012**, *37*, 16346−16358.

(15) Seepersad, D.; Ghouse, J. H.; Adams, T. A., II Dynamic simulation and control of an integrated gasifier/reformer system. Part II: Discrete and model predictive control. *Chem. Eng. Res. Des.* **2015**, *100*, 497−508.

(16) Lao, L.; Aguirre, A.; Tran, A.; Wu, Z.; Durand, H.; Christofides, P. D. CFD Modeling and Control of a Steam Methane Reforming Reactor. *Chem. Eng. Sci.* **2016**, *148*, 78−92.

(17) National Aeronautics and Space Administration, NASA's Viscous Grid Spacing Calculator. http://geolab.larc.nasa.gov/APPS/YPlus/ (accessed 2017).

(18) *ANSYS Fluent Theory Guide 15.0*; ANSYS Inc., 2013.

(19) Xu, J.; Froment, G. F. Methane steam reforming, methanation and water-gas shift: I. Intrinsic kinetics. *AIChE J.* **1989**, *35*, 88−96.

(20) Wesenberg, M. H.; Svendsen, H. F. Mass and heat transfer limitations in a heterogeneous model of a gas-heated steam reformer. *Ind. Eng. Chem. Res.* **2007**, *46*, 667−676.

(21) *Johnson Matthey Catalysts - Delivering world-class hydrogen plant performance*; Johnson Matthey, 2007; http://www.jmcatalysts.cn/en/pdf/HydrogenTechBrochFeb2007.pdf.

(22) Tran, A.; Aguirre, A.; Crose, M.; Durand, H.; Christofides, P. D. Temperature Balancing in Steam Methane Reforming Furnace via an Integrated CFD/Data-Based Optimization Approach. *Comput. Chem. Eng.* **2017**, *104*, 185−200.

(23) Kumar, P. R.; Varaiya, P. *Stochastic Systems: Estimation, Identification, and Adaptive Control*; Prentice-Hall, Inc.: Englewood Cliffs, NJ, 1986.

(24) Rogers, A.; Steiglitz, K. Maximum likelihood estimation of rational transfer function parameters. *IEEE Trans. Autom. Control* **1967**, *12*, 594−597.

(25) Nocedal, J.; Wright, S. J. *Numerical Optimization*, 2nd ed.; Springer Science and Business Media, LLC: New York, NY, 2006.

(26) Axehill, D. Integer Quadratic Programming for Control and Communication. Ph.D. Thesis, Institutionen för systemteknik, 2008.

DOI: 10.1021/acs.iecr.7b00390
Ind. Eng. Chem. Res. 2017, 56, 6002−6011